Appl Phys A (2012) 106:363–376
DOI 10.1007/s00339-011-6693-5

Applied Physics A
Materials Science & Processing

INVITED PAPER

Feasibility study of the application of micro-Raman imaging as complement to micro-XRF imaging

A. Deneckere · B. Vekemans · L. Van de Voorde · P. De Paepe · L. Vincze · L. Moens · P. Vandenabeele

Received: 17 March 2011 / Accepted: 7 November 2011 / Published online: 29 November 2011

Abstract X-ray fluorescence (XRF) spectroscopy and Raman spectroscopy are preferential analytical techniques to study cultural heritage objects, since both techniques may provide complementary information in a non-destructive manner. Moreover, the application of microscopic beams allows the investigation of heterogeneous samples on the microscopic level and the study of the heterogeneity of particular samples. The micro-XRF method became already a routine analytical imaging method also because of the well-established spectrum evaluation methodology enabling specific data handling procedures. These include multivariate statistical analysis procedures such as principal components analysis (PCA) in order to explore and describe the acquired data, and clustering techniques in order to find similar pixels (or areas) in the obtained images. In the case of the micro-Raman technique, however, the usual approach is to perform a single spot analysis of only a few selected positions in order to ultimately identify the material on the basis of the comparison with Raman spectra obtained from reference materials. However, when samples are heterogeneous, imaging is still to be preferred in order to deal with the problem of sampling. With the arrival of a new micro-Raman spectrometer at the UGent laboratories, there was the need to explore the possibilities of Raman imaging. One of the most important aspects of imaging is the time needed for the analysis. Therefore, the influence of different instrumental parameters, such as resolution (low or high) and measuring time per pixel, on the quality of Raman spectra and images was investigated in order to evaluate the possibility of performing fast Raman mappings because of the need to identify the regions of interest on the art object in a more systematic manner.

A. Deneckere (✉) · L. Moens
Research Group Raman Spectroscopy, Department of Analytical Chemistry, Ghent University, Krijgslaan 281, S12, 9000 Ghent, Belgium
e-mail: Raman@UGent.be
Fax: +32-9-2644960

B. Vekemans · L. Van de Voorde · L. Vincze
Research Group X-ray Microspectroscopy and Imaging, Department of Analytical Chemistry, Ghent University, Krijgslaan 281, S12, 9000 Ghent, Belgium

P. De Paepe
Laboratory of Mineralogy and Petrology, Ghent University, Krijgslaan 281, S8, 9000 Ghent, Belgium

P. Vandenabeele
Department of Archaeology, Ghent University, Sint-Pietersnieuwstraat 35, 9000 Ghent, Belgium

1 Introduction

During the last decade, Raman mapping has proved to be a basic tool to gain insight into, among others: the composition of multilayered structures, by investigating stratigraphic samples removed from art objects [1], the deterioration process of pigments in frescos [2], the painting technique of 16th century artists [3], rust scales on archaeological iron artefacts [4] and the penetration depth of conservation treatment on cultural heritage [5]. Non-destructive Raman mapping can be performed using a motorised x–y stage system that allows moving the objects in a plane. When the stage additionally also moves in the z direction, depth profiling can take place. Performing Raman mappings with the conventional experimental set-up may have two limitations: only objects which fit under the microscope can be analysed, and due to the fact that the surfaces of art objects are usually not flat, the analysis is time consuming because of the optimisation of the focal distance that is necessary for each

point [1]. Ropret et al. [1] suggested an alternative experimental set-up to exclude the limitation of the dimensions of the objects: a Raman mapping based on a set of scanning mirrors that direct the laser beam in two spatial directions, vertically through a horizontal exit on the Raman spectrometer. In this approach, when the beam is directed through the microscope objective, the size of the object remains the limiting factor, but when the mirrors are placed at the spectrometer's horizontal exit, considerably larger works of art can be studied, keeping the advantages of full confocality and the possibility to use multiple excitation lines.

In this research, a Raman spectrometer with a conventional experimental set-up is used to perform Raman mappings on a selected area of a porcelain card. Porcelain cards are 19th century art objects, printed by a lithographic process, and are due to their dimensions excellent test-cases for mapping experiments. Next to the Raman mappings also XRF mappings using a conventional set-up were performed on a similar area of the porcelain card. The conventional way of analysing objects with XRF spectroscopy is based on first performing a fast map to select the regions of interest and afterwards performing long point measurements or mappings with a long measurement time in the selected regions of interest [6]. In this work, the possibility of performing fast maps with Raman spectroscopy on a selected area of the porcelain card is evaluated by changing different parameters, such as the measurement time and the resolution.

Porcelain cards are cardboards covered with a layer of leadwhite, printed with text and brightened with decorations. They represent the modern business cards or announcements of the 19th century. Historical details of these cards are described elsewhere [7]. Previous research [7] showed that the identification of the pigments used is straightforward, even when analysing with a short measuring time. Therefore a porcelain card was used as object to evaluate the influence of Raman mapping in high or low resolution mode and measuring for a short or long time.

Before presenting the results of the XRF maps and discussing the influence of the different parameters on the Raman maps, an overview of the development and applications in the field of archaeometry of Raman spectroscopy, XRF spectroscopy and the combination of both techniques is given.

2 Techniques

2.1 Raman spectroscopy

During the last 15 years Raman spectroscopy has increasingly been applied for the analysis of art objects [8, 9]. In 1979 Dhamelincourt et al. [10] described the coupling of a microscope to the Raman spectrometer and the application for the analysis of art objects. The earliest papers focussed in general on instrumental improvements and explored the suitability of the approach for the investigation of art objects [11, 12], focussing mainly on pigment identification. The identification of pigments in art objects can provide information on the manufacture date [13], can help to decide on future restoration actions [14], or can be useful to expose forgeries [13, 15]. Pigment analysis with Raman spectroscopy has been performed to study different types of art objects [16].

A small number of studies were carried out on antique polychrome objects, such as dynastic Egyptian funerary artefacts [17] and wooden crucifixes [15].

Panel paintings [18–20], rock paintings [21–23] and wall paintings [24–26] are also common objects to analyse using Raman spectroscopy. When investigating art objects the focus is often not only on the identification of pigments, but also on the identification of deterioration products [27], such as salts [28] that are formed by weathering processes. Identification of deterioration products can provide conservators information on the future protection of the object.

Raman spectroscopic analysis of manuscripts has mainly been concerned with pigment investigation of European mediaeval books of loose parchment leaves [29–31], but also extends to other periods. Next to pigment identification, Raman spectroscopic analysis of manuscripts can give insight in relations between manuscripts and scriptoria [32]. An extended research of different manuscripts can lead to an overview of pigments used over a wider period or region.

Research was done on works of paper such as lithographs [33–35], drawings [36] and wallpapers [37–39]. Analysis of these works of art should be undertaken with special care, since these art objects are extremely vulnerable to damage.

For Raman spectroscopy, and similarly to all other analytical techniques, the evolution in applications is directly linked to the improvements in instrument technology. One of the most important instrumental improvements is the presence of the capability to measure different layers in confocal mode, and the resulted effective spatial resolution achieved in the instruments [16].

Using standard micro-Raman equipment, the direct analysis of large art objects is difficult since focussing the laser beam on the surface of the artwork is not easy. An elegant solution for this problem is using fibre optics to send the laser beam to the artefact and to collect the backscattered radiation [40]. Due to the development of mobile equipment [41], *in situ* analysis, where the instrument is transported to the location of the art object, could be executed.

During the last decade motorised stages were introduced, which can move an object point by point in three dimensions. Due to this instrumental development, Raman spectroscopy can be used as a mapping technique. Mapping an

art object consists of performing point measurements for scanning the art object in two or three dimensions. The most important disadvantage of mapping is that it is very time consuming, because of the sequential analysis. A solution for this problem is performing Raman imaging. With this technique a larger area of the sample is illuminated and the spectral information is gathered on different places of the detector. The disadvantage of this technique is that only the total intensity within a certain wavelength region is recorded. As a consequence, no background correction can be made and apart from the total intensity no other variables, such as band position or bandwidth, could be plotted.

In 1990, Bowden et al. [42] presented a new approach: line scanning. In this approach a line is illuminated on the sample instead of a single point. This approach increases the speed of data acquisition, while good spectral quality is maintained. In 2008, Renishaw [43] developed a commercial Raman spectrometer based on this approach, the Streamline plus. The instrument uses optics within the inVia Raman microscope to illuminate a line on the sample. The inVia's motorised microscope stage moves the sample beneath the objective lens so that the line is rasterised across the region of interest. Data are swept synchronously across the detector as the line moves across the sample, and are read out simultaneously.

Micro-Raman mapping results in a multivariate data set. Information on the chemical composition of a sample can be obtained by multivariate analysis [3, 44, 45]. The most commonly used techniques for multivariate analysis are: principal components analysis (PCA), partial least squares regression (PLSR), hierarchical cluster analysis (HCA), K-means cluster analysis (KCA) and fuzzy cluster analysis (FCA). PCA reduces the number of variables condensing all the spectral information of a large number of spectra into a few latent variables (principle components). For PLSR a reference data set consisting of spectra with known analyte concentrations is used to build a calibration model. In cluster analysis, HCA, KCA and FCA, spectra are segmented in groups (clusters) according to their similarity, so that all spectra belonging to one cluster have similar characteristics. The difference between HCA and KCA is that for KCA the number of clusters should be known in advance. In "hard" clustering methods such as HCA, a spectrum exclusively belongs to one cluster, whereas "soft" methods such as FCA allow one spectrum to belong to more than one cluster at the same time.

2.2 X-ray fluorescence (XRF) spectroscopy

The first application of XRF in the field of archaeology was in 1967, when Vilnat et al. [46] compared different XRF methods for the analysis of enamel. During the next 20 years the use of XRF spectrometry for the analysis of art objects was only for a few cases reported in scientific literature, among others: for the analysis of Etruscan gold objects (1973) [47], pigments of Minoan painted pottery (1979) [48], online analysis of china clays (1982) [49], quantitative analysis of traces of barium in porcelains (1985) [50] and archaeological pottery (1987) [51]. The small number of applications is probably due to instrumental drawbacks.

Starting from the 1990s, the number of applications of XRF spectroscopy for the analysis of art increases exponentially because of instrumental developments. In 1976 Cesareo et al. [52] already mentioned the use of portable units for analysis with XRF spectroscopy. This was followed by the discussion to use different probes for the analysis of art objects by Vaughan [53] in 1982. In 1998 Longoni et al. [54] introduced a portable XRF spectrometer for non-destructive analysis in archaeometry. Until now, the detectors used in conventional XRF spectrometers were the classical high-resolution cryogenic detectors, like Si(Li) and HPGe detectors (whose resolution is in the order of 140 eV FWHM at 6 keV). These detectors are not completely suitable for portable instrumentation because of the necessary cooling with liquid N_2. To compensate for this disadvantage, non-cryogenic detectors, like Peltier cooled Si PIN diodes, have been developed, with a big improvement in terms of size and weight of the instrumentation [55]. The energy resolution of this type of detectors of the order of 250 eV FWHM at 6 keV, is nevertheless sometimes unsatisfactory. This type of portable XRF spectrometer was used for the analysis of metal alloys, pottery and pigment identification in paintings [56]. The same type of instrument was used for the analysis of Egyptian statues in the Museum Vleeshuis (Antwerp, Belgium) [57]. This instrument has in addition a mini-focus side window X-ray tube, which implies the use of a small beam with a spot size of approximately 0.5 mm^2.

Williams-Thorpe et al. [58] introduced the use of aHgI detector for the analysis of British Stone Axe. Nevertheless, the developed portable XRF spectrometers use detectors that need cooling: a liquid N_2 cooled Si(Li) detector (X-art [59]), a Peltier cooled Si-PIN X-ray detector (semi-micro XRF spectrometer [60]) or a Peltier cooled Si drift detector (Labview controlled portable XRF spectrometer [61]). The selection of the detector for the analysis of art objects depends on the nature of the object and the characteristics of the environment [62].

These instrumental developments made portable XRF spectroscopy an appropriate technique for qualitative (*in situ*) analysis of art objects, such as pigment analysis of Spanish artworks [63], enamels [64] and pigments analysis of rock art [65].

Performing quantitative analysis requires the use of an excitation beam with a very stable energy and intensity. This is essential for the determination of elemental concentrations since it simplifies the calibration procedures.

A portable XRF spectrometer was introduced for this purpose: the BSC-XRF system [66] (beam stability controlled XRF spectrometer). This spectrometer is equipped with a system to monitor the energy and stability of the beam emitted by the X-ray tube. The control of the system is obtained by a direct intervention on the beam through suitable parameters. In order to operate under stable conditions, the system was accurately calibrated. This spectrometer was used for the quantitative analysis of archaeological pottery [67].

In the last decade, many instrumental analytical techniques have developed microscopic equivalents. The drive for this development is twofold: the need to improve the techniques to be able to investigate the higher degree of material complexity, and the growing need to investigate local changes in properties of materials. For this reason, portable micro-XRF spectrometers [68, 69] were introduced for the analysis of art objects. Bunzanich et al. [70, 71] reported the use of a portable micro-X-ray fluorescence spectrometer with polycapillary optics and vacuum chamber for archaeometrical and other applications. When working in vacuum, the detection of low Z elements is possible. This instrument was used for the identification of Egyptian blue ($CaCuSi_4O_{10}$) in art objects of the Egyptian collection of the Kunsthistorisches Museum in Vienna, Austria [72]. Normally the detection of Ca and Si is difficult, but with this device also the presence of Si (low Z element) can be easily detected. The presence of Si is important to distinguish between the blue pigments azurite ($2CuCO_3{\cdot}Cu(OH)_2$) and Egyptian blue ($CaCuSi_4O_{10}$).

In all the above-mentioned applications of XRF spectroscopy for the analysis of art or archaeological objects, the microscopic X-ray beam has been used to perform local analysis by point measurements, 2D elemental mapping [73, 74] or line-scanning on the sample surface, but not to perform investigations in depth. In 2003, a 3D micro-XRF analysis set-up was introduced to perform depth-sensitive investigations of paint layers in ancient Indian Mughal miniatures [75]. Successive paint layers could be distinguished with a depth resolution of about 10 µm. This set-up was also used for the depth resolved investigation of corrosion layers of historical glass objects [76]. Until now monochromatic 3D micro-XRF is only possible using synchrotron radiation, as X-ray tube radiation in combination with state-of-the-art monochromatising optics does not yield enough flux on the sample. Using a polychromatic set-up in combination with a conventional X-ray tube results in an increase of the flux on the sample. By using this set-up, compact XRF spectrometers can be developed for archaeometric applications [77].

2.3 Combined techniques

Using a combination of analytical techniques has the advantage that complementary information could be gathered. In this research, Raman spectroscopy gives molecular information, while XRF spectroscopy provides elemental information on the pigments used.

Hunter et al. [78] described the first application of a combined approach for the analysis of archaeological art objects in 1993. They used a combination of XRF spectroscopy, Raman spectroscopy, electron spin resonance, infrared spectroscopy, thermogravimetric analysis, scanning electron microscopy and X-radiography. During the last decade, such very extended approaches were used for the analyses of: sienese 'archaic' majolica [79], Byzantine wall paintings [80] and the tomb of Menna, Theban Necropolis, Egypt [81]. Nevertheless, typically many archaeometric analyses were performed using a combination of only three techniques: (a) combination of infrared (IR), Raman and XRF spectroscopy for the analysis of inks [82, 83], English polychrome alabaster sculptures [84], ancient pottery [85] and ancient polychrome prints [86]; (b) combination of scanning electron microscopy, Raman and XRF spectroscopy for the analysis of Perugino's palette [87], an ancient Italian manuscript [88], a painted leather screen [89] and for the identification of 19th and 20th century pigments [90]; (c) combination of Nuclear Magnetic Resonance (NMR), Raman and XRF spectroscopy for the analysis of coloured maps [91, 92], and (d) combination of X-ray diffraction, Raman and XRF spectroscopy for the analysis of Chinese celadon shards [93] and illuminated manuscripts [94].

The current research focusses on the combination of Raman spectroscopy with XRF spectroscopy, because both instruments are readily available in the UGent Department of Analytical Chemistry.

During the last decade the combination of these two techniques was applied for the analysis of different art objects, such as: mural paintings [95–97], Byzantine icons [98], wallpaper [99], canvas painting [18], Spanish stamps [100], Islamic manuscripts [101] and blue glaze [102].

A combination of a portable Raman spectrometer with a portable XRF spectrometer was used to monitor the influence of nitrate on historical building materials [103, 104]. Depending on the nature of the materials and the nitrate compound impacting them, several nitrate salts can be formed: $NaNO_3$, $Mg(NO_3)_2$, $Ca(NO_3)_2$ and $Ba(NO_3)_2$. Since with Raman spectroscopy only the strongest band of the nitrates (1060–1035 cm^{-1}) is detectable, XRF spectroscopy helps to distinguish between the different nitrates, based on the detectable elements present in these salts (Na, Mg, Ca, Ba).

Ramos et al. [105] reported the use of a special data treatment for the classification of ochre pigments, where Raman and XRF data are fused. If different spectroscopic techniques are used, the spectra need to be balanced in order to perform a correct data sensor association. Several methods

could be used, but in this case study they make use of partial least square discriminant analysis (PLS-DA).

All the above-mentioned analyses were based on point measurements. In many cases there is also an interest to make maps of the analysed object. In an earlier study [73] we already reported the use of a two-dimensional XRF mapping to get a better insight in the restoration processes the painting underwent during history.

3 Experimental

The porcelain card (Fig. 1) selected for this research represents a typical business card: FransClaes, manufacturer of chemical products in Ghent, Belgium. This card was produced at a local lithographic shop: G. Jacqmain and R. Basse. The dimensions of the card are: 133 × 89 × 1 mm.

3.1 Instrumentation

3.1.1 Confocal micro-Raman spectroscopy

The laboratory Raman spectrometer used is a Bruker Optics 'Senterra' dispersive Raman spectrometer with a BX51 microscope. The Raman spectrometer is equipped with 532 (Nd:YAG) and 785 nm (diode) laser sources. High resolution spectra are recorded in 3 spectral windows, covering the 60–3700 cm^{-1} and 80–3500 cm^{-1} for the 532 and 785 nm laser, respectively. The system uses a thermoelectrically cooled CCD detector, operating at −65°C. Five software-controlled settings for the power of each laser are available: 100, 50, 25, 10 and 1%, i.e. up to ca 35 mW at the sample for the 785 nm laser. The microscope has 5×, 20× and 50× objectives, with spot sizes of approximately 50, 10 and 4 µm, respectively. The microscope contains a joystick-controlled motorised stage and setting the analysis area is accomplished with the aid of an attached video camera. The instrument is controlled via the OPUS software version 6.5.6. Mapping the selected area of the porcelain card was performed using the 785 nm laser at 1% power setting, to avoid any possible sample damage.

3.1.2 Energy dispersive X-ray fluorescence spectroscopy (EDXRF)

A laboratory micro-XRF system (Eagle-III microprobe, EDAX, Inc., Mahwah, NJ, USA) provided elemental information of the mapped area. This spectrometer is equipped with a microfocus X-ray tube with an Rh anode, a polycapillary lens (X-ray Optical Systems, Inc., NY, USA) for X-ray focussing, and a N_2 cooled 80 mm^2 energy dispersive Si-(Li) detector. The sample chamber incorporates an XYZ motorised stage for sample positioning. A high resolution microscope is used to position the sample on the desired distance from the polycapillary. Operating in vacuum allows the use of the Rh-L photons originating from the X-ray tube to improve the investigation of low Z-elements down to sodium. Mapping of the selected area of the porcelain card was performed at an operating X-ray tube voltage of 40 kV, a tube current of 80 µA to optimise the detection of X-rays corresponding to ca. 30% detector dead time, and a spot size of 100 µm on the sample.

Fig. 1 Picture of the analysed porcelain card (133 × 89 × 1 mm), with selected region of interest

4 Results and discussion

4.1 X-ray fluorescence spectroscopy (XRF)

In the first step of this research the possibility to identify the different pigments used was explored performing a fast map with XRF spectroscopy. The resulting images were used to select an area on the card to perform a second map with a longer measurement time. On this second map principal components analysis (PCA) and *K*-means cluster analysis were performed.

4.1.1 Identification of the pigments

For the first map an area of 18,923 by 13,563 µm was mapped. In this area, respectively 128 × 100 single points were measured in vacuum for a very short time (0.5 s). Although a short measurement time of 0.5 s was chosen, approximately two hours were needed to acquire these data. This preliminary map was performed to select the area of interest of the porcelain card.

The results of this map are presented in Fig. 2. This fast mapping already provides a lot of information on the elements of the pigments used. The maps of Al-K and Si-K lines (Fig. 2) are very similar. The most intense regions of both lines cover the blue zones of the selected area. The presence of Al and Si may indicate that ultramarine blue ($Na_{8-10}Al_6Si_6O_{24}S_{2-4}$) was used as blue pigment. The maps of Hg-L, M and S-K are also very similar. This implies that for the red regions, vermilion (HgS) was used as red pigment. If we take a closer look at the X-ray map of Pb-L and Pb-M, we can recognise the whole structure of the selected area in the map. This probably means that the whole cardboard is covered with a layer of lead white. For the green zones of the card, the X-ray signal of Cu-K is the most intense. This suggests that a Cu-based pigment was used as green pigment. The XRF results of this fast map already give some information of the elements used for the golden, brown colour: a mixture of Cu and Zn.

These first results allowed the selection of a sub-area of 8 by 8 mm (red raster in Fig. 2) for the next imaging experiment. For this, each of the 64 × 64 single points were measured for 10 s. The total map of the area took approximately 17 hours. On this XRF data set some multivariate statistical techniques were performed, to see if even better XRF maps could be obtained.

4.1.2 Chemometrical data processing

Principal components analysis (PCA) This XRF data set, which consists of series of X-ray maps, each corresponding to one chemical element, may contain maps which are highly correlated (e.g. Fig. 3, Hg and S maps). Figure 4 shows the principal component maps resulting from the PCA of the data set presented in Fig. 3. Principal components analysis (PCA) is a multivariate statistical technique

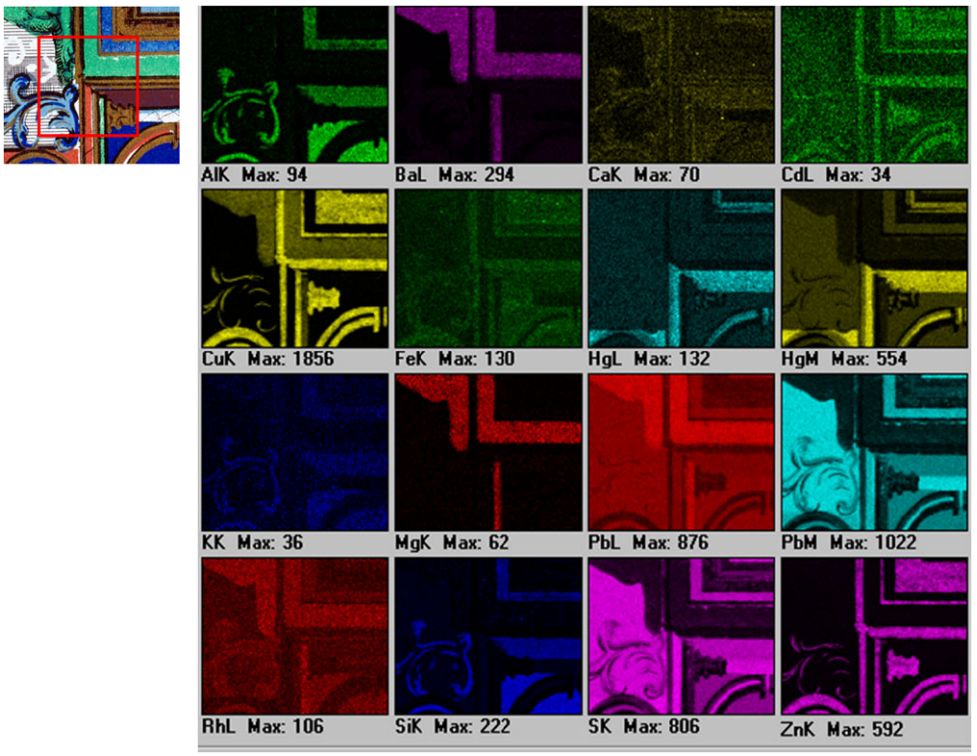

Fig. 2 µ-XRF elemental maps obtained by scanning the selected area of the porcelain card using a 100 µm X-ray beam derived from an Rh anode operated at 40 kV. Step size, 0.149 × 0.137 mm, image size 128 × 100 pixels, or 18.923 × 13.563 mm; spectrum collection time per pixel, 0.5 s (2 hours)

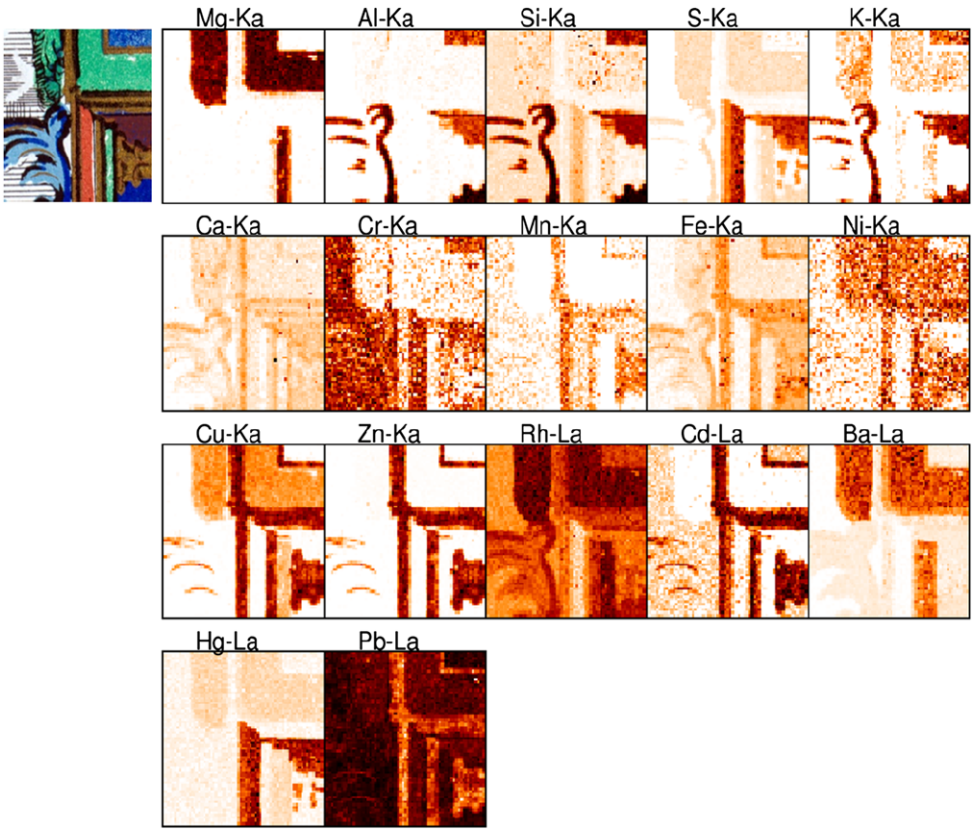

Fig. 3 µ-XRF elemental maps obtained by scanning the selected area of the porcelain card using a 100 µm X-ray beam derived from an Rh anode operated at 40 kV. Step size, 0.125 × 0.125 mm, image size 65 × 65 pixels, or 8 × 8 mm; spectrum collection time per pixel, 10 s (17 hours)

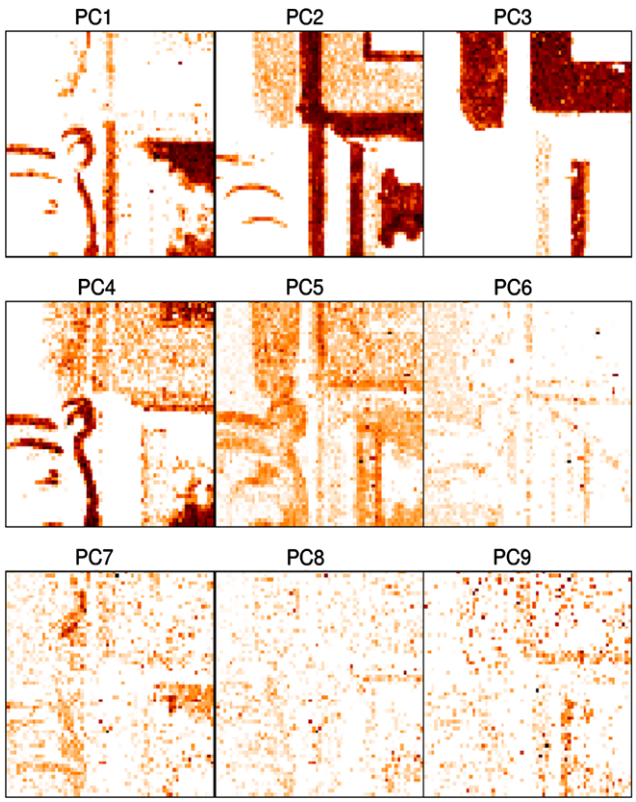

Fig. 4 Score images obtained by PCA of the X-ray maps in Fig. 3

which aims to detect similarities between experimental multivariate data sets, essentially through reduction of the dimensionality of the data. In Fig. 5(a) the contribution to the variance (CVE) of each PC is plotted; clearly the first six PCs explain 90% of the total variance in the data set. Figure 5(b) shows the PC2-PC3 loadings plot of the original variables, i.e. the chemical elements. In the loadings plot the presence of vermilion is clearly visible (correlation between Hg-La and S-Ka). The loadings plot also shows a correlation between Al-Ka, Si-Ka and K-Ka. This correlation may indicate the presence of ultramarine blue. For the correlation between Mg-Ka and Ba-La on the one side, and between Fe-Ka and Zn-Ka on the other side, we do not have a plausible explanation. Perhaps the correlation between Fe-Ka and Zn-Ka is due to the lithographical process: for the ink a combination of Fe and Zn was often used. Mg and Ba are chemically related and therefore appear often together.

K-means cluster analysis All clustering methods are based on measuring the degree of similarity between two of the objects to be clustered. The K-means cluster algorithm is an iterative procedure that derives its name from the fact that it assumes the final number of object classes to be known a priori and equal to K. It would be straightforward that K is equal to the number of meaningful principal components. However, in practice it is difficult to define the number of important principal components.

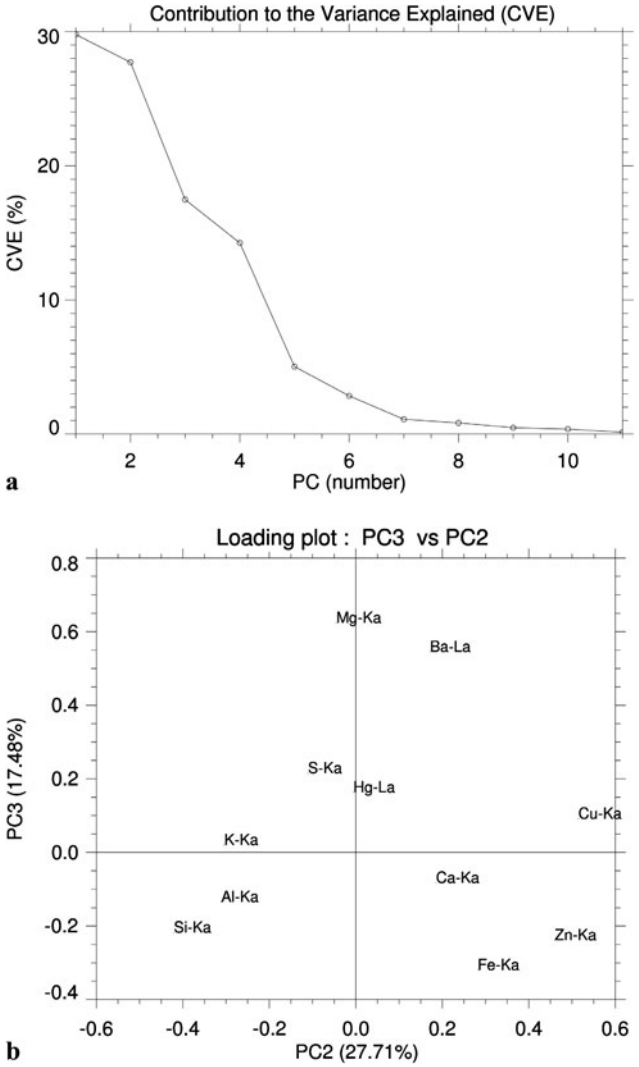

Fig. 5 Scatter plot corresponding to the data shown in Fig. 4: (**a**) CVE (contribution of variance explained) of each principal component and (**b**) loading plot in the PC2-PC3 plane

Therefore, for practical considerations, a K-means clustering with $K = 15$, a somewhat arbitrarily and too high value, was chosen. The resulting clusters represent sub-areas of the obtained image. Comparing these cluster images with the optical image (picture) of the selected area, gives elemental information on the pigments used. The clusters obtained by applying the K-means algorithm to the original data are shown in Fig. 6. Figure 7(a) shows the sum spectrum and the cluster image of the white zones of the analysed area. The presence of the intense Pb-L lines in the sum spectrum indicate that lead white ($2PbCO_3{\cdot}Pb(OH)_2$) was used for the covering layer of the cardboard. The sum spectrum of Fig. 7(b) shows intense Cu-K lines, suggesting that a Cu-based pigment was used for the green zones. For the blue pigment (Fig. 7(c)), the Al-K, Si-K and the S-K lines can be observed in the sum spectrum. Also for the red pigment (Fig. 7(d)), the intense Hg-L and S-K lines are clearly visible in the sum spectrum. Performing K-means cluster analysis on the XRF data set delivers additional information on the different types of brown colours used. Figure 7(e) shows intense Hg-L and Cu-K lines. This suggests that a mixture of vermilion and a Cu-based pigment was used for the dark brown colour. The brown, bronze colour is also a mixture of vermilion and a Cu-based pigment (Fig. 7(f)), but some Zn was also applied to the mixture.

Due to the penetrative character of the X-rays, XRF spectroscopy delivers spectral data that contain information of all layers in case of multilayer samples. Additional XRF spectroscopy only delivers elemental information, which makes in some cases identification of the pigments impossible.

4.2 Raman spectroscopy

For the Raman analysis of the porcelain cards, approximately the same area was mapped as during the XRF analysis. In a first step of the Raman the analysis point measurements (60 s, 10 acc) were performed in order to identify the different pigments used. This first step was necessary to select the Raman wavenumbers specific for each identified pigment. These wavenumbers are necessary to create an image of the selected area of the porcelain card. In a second step of the Raman analysis the influence of the measuring time and measuring in high and low resolution modes on the intensity of the selected Raman wavenumbers was evaluated, in order to decide whether a fast mapping can be used to select the region of interest of art objects.

4.2.1 Identification of the pigments

For the identification of the pigments used, point measurements were performed in the same area which was mapped with XRF spectroscopy. Table 1 gives an overview of the identified pigments with Raman spectroscopy and the identified elements with XRF spectroscopy for each colour. After the selection of the Raman wavenumbers of interest, a selected area of 8.031×5.658 mm (81×56 points) (Fig. 8(a)) was mapped with the red laser (785 nm), with a laser power of 1% (0.63 mW). A $5\times$ objective lens was used, resulting in a spot size of ca. 50 µm on the card. The measurement time of all the single points of the mapping was 60 s (20 s, 3 acc), resulting in a total time of almost 7 days for the whole mapped area. These 7 days are the accumulated result of the measurements, the movement of the sample, the movement of the grating to record different spectral regions, and the automatic background correction of the used Raman spectrometer. The control software OPUS 6.5.6 (Bruker) is not able to switch off the automatic background correction, which results in a doubling of the measurement time.

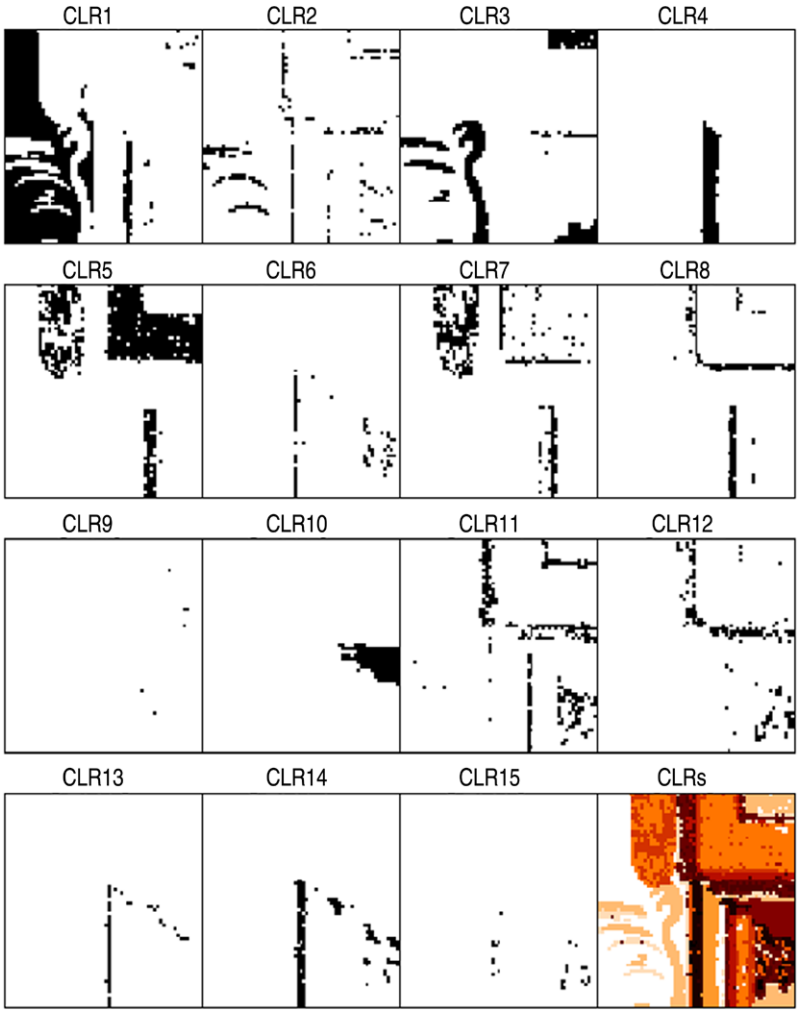

Fig. 6 Compound segmentation masks obtained by *K*-means clustering of the original data

To construct the maps of the different pigments, the data were processed with OPUS 6.5.6. A selection of the most intense bands was made for the identified pigments: lead white (1050 cm^{-1}), vermilion (254 cm^{-1}) and ultramarine blue (545 cm^{-1}). The Raman signal for malachite (218 cm^{-1}) and carbon black (1297 cm^{-1}) were too weak to give a clear image. A possible solution for this problem could be performing the same mapping with the green laser (532 nm). Next, all the selected bands were integrated one by one. For this, first the baseline is constructed before integration of the surface area of the Raman band above the baseline. The results of this integration are presented in Fig. 8.

Figure 8(b) shows the integration of the most intense band of lead white (1050 cm^{-1}). One can see that lead white is detected over the whole mapped area, which implies that the first step in the manufacturing process was covering the cardboard with a layer of lead white. The different intensities of the Raman signal of lead white on the different coloured areas are also clearly visible. The maps made by the integration of the bands of vermilion (Fig. 8(c)) and ultramarine blue (Fig. 8(d)) show obviously the red and blue coloured zones of the mapped area.

4.2.2 The influence of spectral resolution and measurement time

To evaluate the dependency of the resolution on the intensity of the Raman signal, a similar area of the porcelain card (the red frame in Fig. 8(a)) was mapped two times with the same experimental parameters (20 s, 3 acc, 5× objective lens), except for the spectral resolution. The first map was performed using the high spectral resolution mode (3–5 cm^{-1}), while the second map was recorded in low spectral resolution mode (9–18 cm^{-1}). Changing to lower resolution results for the used Raman spectrometer in a significantly shorter measurement time, because the spectra are recorded using one grating over a range of 90–3500 cm^{-1}. When measuring in high resolution mode the grating has to turn during the measurement, because the two spectral ranges (80–1525 and 1520–2660 cm^{-1}) are measured separately and stitched together. This results in a much longer

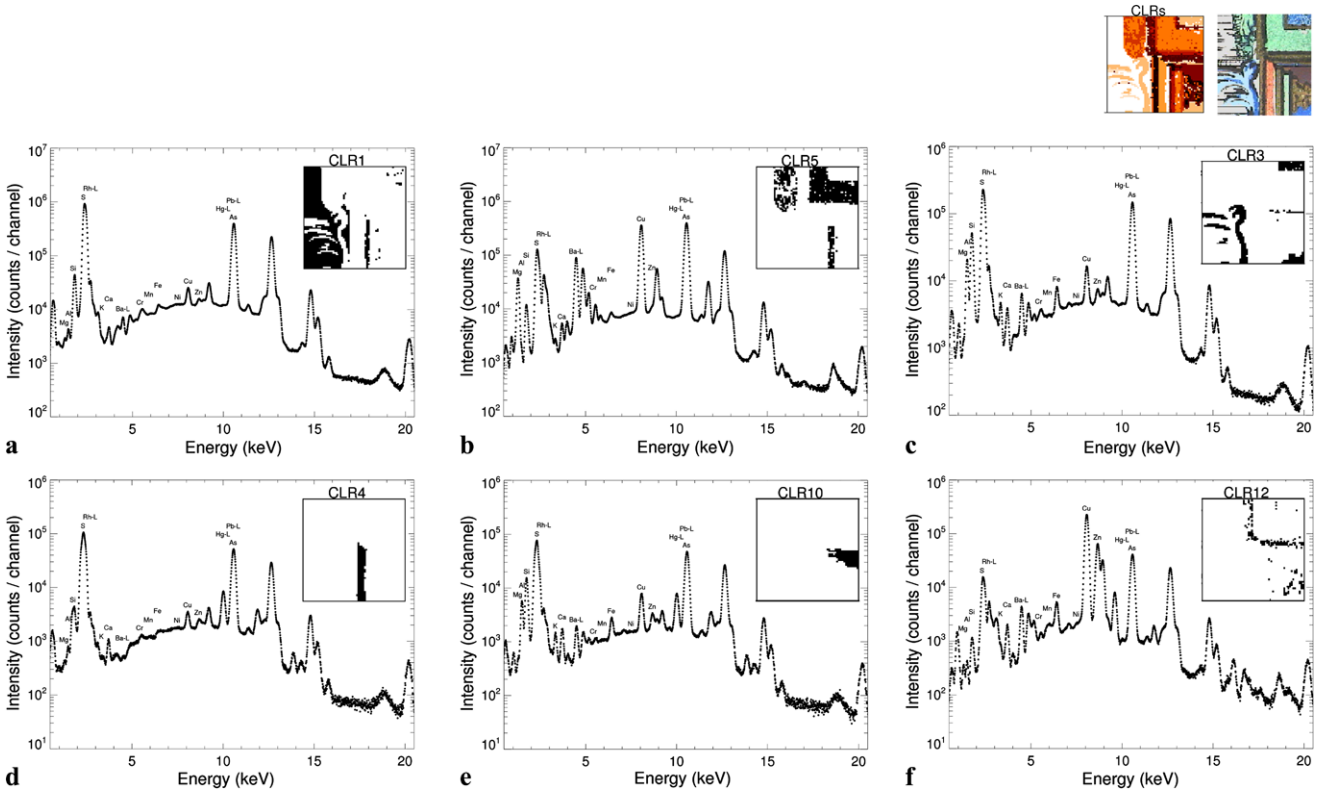

Fig. 7 Sum spectra of the different clusters showing the presence of: (**a**) lead white for the *white colour*, (**b**) a Cu-based pigment for the *green colour*, (**c**) ultramarine blue for the *dark blue colour*, (**d**) vermilion for the *red colour*, (**e**) a mixture of vermilion and a Cu-based pigment for the *dark brown colour*, and (**f**) a mixture of vermilion, a Cu-based and a Zn-based pigment for the *light brown*, *bronze colour*

Table 1 Overview of the identified pigments with Raman spectroscopy and the identified elements with XRF spectroscopy for each colour

Colour	XRF results	Raman results
White	Pb	Lead white ($2PbCO_3{\cdot}Pb(OH)_2$)
Red	Hg, S	Vermilion (HgS)
Blue	Al, Si, S	Ultramarine blue ($Na_{8-10}Al_6Si_6O_{24}S_{2-4}$)
Green	Cu	Malachite ($CuCO_3{\cdot}Cu(OH)_2$)
Black	/	Carbon black (C)
Brown, gold	Cu, Hg, S, Zn	/
	Cu, Hg, S	/

measurement time, especially because after each movement of the grating the spectrometer performs a new calibration. The total mapping time of the map with low resolution was ca. 22 hours, while for the map with high resolution the total mapping time was ca. 7 days.

As part of the interpretation of the Raman data, an in-house written software was developed. This program automatically removes the spectral background using the SNIP method [106]. Next, the sum spectrum of all the spectra is made and the Raman bands are selected. In a following step the selected bands are integrated for all spectra. Details of this in-house written software will be published elsewere [107]. By selection of one band, the distribution of the Raman intensity over the selected area can be shown as a map. Figure 9 compares different Raman maps with high and low resolution. Figures 9 shows the Raman intensity of the band of lead white at ca. 1050 cm^{-1}, with respectively high (Fig. 9(a)) and low (Fig. 9(b)) spectral resolution. The Raman map with low spectral resolution gives a better view of the whole structure of the porcelain card than measuring in high resolution mode. The same comparison is made for the Raman band of vermilion at 254 cm^{-1}. The Raman map with low spectral resolution (Fig. 9(d)) is again more obvious than the one with high spectral resolution (Fig. 9(c)). When measuring in low spectral resolution mode, the amount of light which enters the detector is

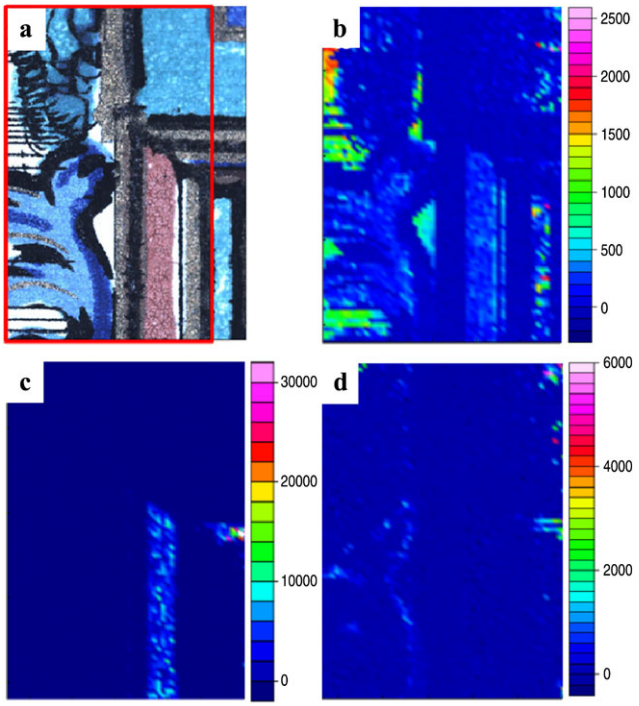

Fig. 8 (**a**) Optical microscope image of the analysed area of the porcelain card, integration of the Raman band at (**b**) 1050 cm^{-1} (*lead white*), (**c**) 257 cm^{-1} (*vermilion*) and (**d**) 545 cm^{-1} (*ultramarine blue*). (785 nm, 5× objective, 20 s, 3 acc, high spectral resolution, 1% laser power)

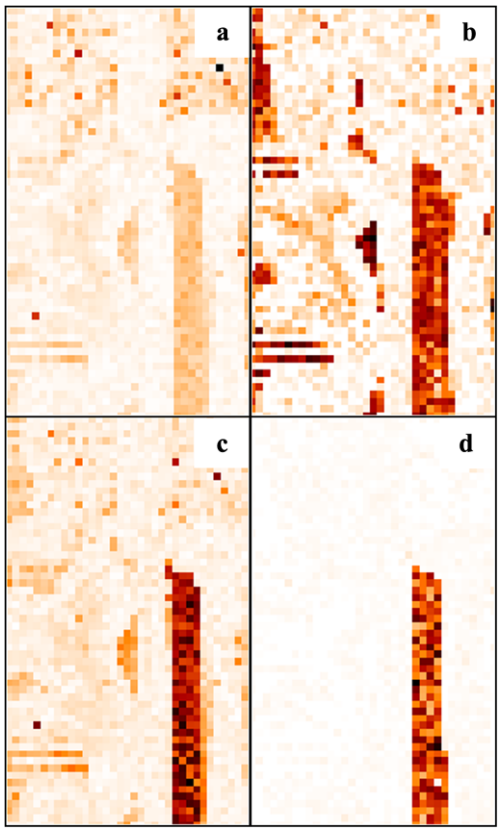

Fig. 9 Map of the Raman intensity of: lead white at 1050 cm^{-1} for (**a**) high and (**b**) low spectral resolution; and vermilion at 254 cm^{-1} for (**c**) high and (**d**) low spectral resolution. (785 nm, 5× objective, 20 s, 3 acc, 1% laser power)

higher, corresponding to a higher sensitivity. By measuring at low spectral resolution, the same information on the pigments is obtained in a shorter period. In this particular example the measurement time was reduced with a factor of ca. 7. This reduction of the measurement time is, when measuring with the Senterra Raman spectrometer, important because of the instability of the stage.

The same procedure was followed to evaluate the influence of the measurement time on the quality of the map. The same area of the porcelain card was twice mapped with the same experimental parameters (5× objective lens, low resolution), but with different measurement times. For the first map the measurement time of a single point spectrum was 60 s (20 s, 3 acc), while for the second map the measurement time only was 6 s (3 s, 2 acc). The total time of the long measurement was ca. 22 hours and for the short measurement ca. 6 hours. Figure 10 shows the different Raman maps: the intensity of the Raman band of lead white at 1050 cm^{-1} for a long (Fig. 10(a)) and a short measurements (Fig. 10(b)); and the intensity of the Raman band of vermilion at 254 cm^{-1} for a long (Fig. 10(c)) and a short measurements (Fig. 10(d)). Only the Raman maps of lead white and vermilion are showed, because for the other pigments there is no clear difference between the maps under different circumstances. This is because of the low signal-to-noise ratio of the Raman data, due to the instability of the stage system for long measurements. The instability of the stage is a drawback in this research. It is obvious that with a stable stage, longer measurements would lead to better Raman maps.

The Raman maps of the long measurements (Fig. 10(a) and (c)) are sharper than the ones of the short measurement. We can conclude that we have to select a (longer) measurement time, which gives a more obvious Raman signal. Choosing a shorter measurement time has in this case no advantages.

Due to the weak Raman signal, noisy Raman images were obtained. These noisy images eventuate, after performing multivariate statistical analysis such as PCA and K-means cluster analysis, in noisy results. To improve these results Raman images with better signal-to-noise ratio have to be obtained.

5 Conclusions

This paper shows that by mapping an art object with Raman spectroscopy and XRF spectroscopy, molecular and elemental images could be produced containing information on the

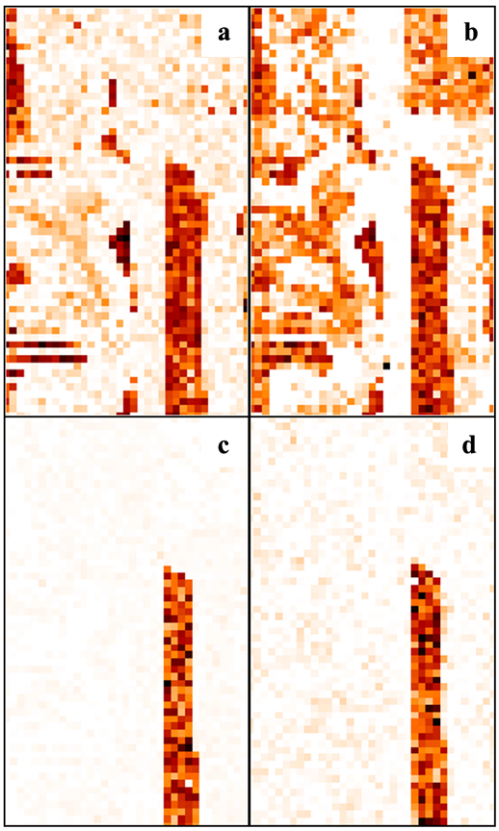

Fig. 10 Raman map of the Raman intensity of: lead white at 1050 cm^{-1} for (**a**) long (20 s, 3 acc) and (**b**) short (3 s, 2 acc) measurement time; and vermilion at 254 cm^{-1} for (**c**) long and (**d**) short measurement time. (785 nm, 5× objective, low resolution, 1% laser power)

pigments used: ultramarine blue, vermilion, malachite, carbon black and lead white.

By using the obtained XRF data set, the possibility of using principal components analysis (PCA) and K-means cluster analysis for gathering information on the pigments used, has been explored. After performing K-means cluster analysis on the data set, the resulting sum spectra associated with each image segment give additional information and simplify the interpretation of the measurements.

It was also indicated that by recording Raman maps at low spectral resolution a similar image was obtained as by measuring at high resolution. This results in a shorter time needed for analysing the art object.

In the future we intend to examine if the total measurement time for the Raman analysis could be diminished by using a stable stage and if the new control software is mandatory to allow auto-focussing without the automatic calibration, in order to improve the quality and reduce the time.

Acknowledgements This work is supported by the BELSPO Interuniversity Attraction Pole Program P6/16 (Belgium).

References

1. P. Ropret, C. Miliani, S.A. Centeno, C. Tavzes, F. Rosi, J. Raman Spectrosc. **41**, 1172 (2010)
2. S. Aze, J.M. Vallet, A. Baronnet, O. Grauby, Eur. J. Mineral. **18**, 835 (2006)
3. D. Lau, C. Villis, S. Furman, M. Livett, Anal. Chim. Acta **610**, 15 (2008)
4. D. Neff, L. Bellot-Gurlet, P. Dillmann, S. Reguer, L. Legrand, J. Raman Spectrosc. **37**, 1228 (2006)
5. C. Conti, C. Colombo, M. Matteini, M. Realini, G. Zerbi, J. Raman Spectrosc. **41**, 1254 (2010)
6. B. Vekemans, K. Janssens, L. Vincze, A. Aerts, F. Adams, J. Hertogen, X-Ray Spectrom. **26**, 333 (1997)
7. P. Vandenabeele, P. De Paepe, L. Moens, J. Raman Spectrosc. **39**, 1099 (2008)
8. P. Vandenabeele, L. Moens, *Overview: Raman Spectroscopy of Pigments and Dyes* (Royal Soc Chemistry, Cambridge, 2005)
9. G.D. Smith, R.J.H. Clark, Journal of Archaeological. Science **31**, 1137 (2004)
10. P. Dhamelincourt, F. Wallart, M. Leclercq, A.T. Nguyen, D.O. Landon, Anal. Chem. **51**, A414 (1979)
11. B. Guineau, J. Forensic Sci. **29**, 471 (1984)
12. B. Guineau, J. Vezin, Scriptorium **46**, 224 (1992)
13. S. Saverwyns, J. Raman Spectrosc. **41**, 1235 (2010)
14. I. Martinez-Arkarazo, A. Sarmiento, M. Maguregui, K. Castro, J.M. Madariaga, Anal. Bioanal. Chem. **397**, 2717 (2010)
15. S.A. Centeno, D. Mahon, M.T. Wypyski, J. Raman Spectrosc. **35**, 774 (2004)
16. P. Vandenabeele, H.G.M. Edwards, L. Moens, Chem. Rev. **107**, 675 (2007)
17. H.G.M. Edwards, S.E.J. Villar, K.A. Eremin, J. Raman Spectrosc. **35**, 786 (2004)
18. I. Borgia, B.G. Brunetti, C. Miliani, C. Ricci, C. Seccaroni, A. Sgamellotti, J. Cult. Heritage **8**, 65 (2007)
19. P. Vandenabeele, K. Castro, M. Hargreaves, L. Moens, J.M. Madariaga, H.G.M. Edwards, Anal. Chim. Acta **588**, 108 (2007)
20. D. Marano, M. Marniontelli, G.E. De Benedetto, I.M. Catalano, L. Sabbatini, F. Vona, *Pigment Identification on "The Ecstasy of St. Theresa" Painting by Raman Microscopy* (Springer, Berlin, 2007)
21. D.C. Smith, M. Bouchard, M. Lorblanchet, J. Raman Spectrosc. **30**, 347 (1999)
22. R.A. Goodall, B. David, P. Kershaw, P.M. Fredericks, Journal of Archaeological. Science **36**, 2617 (2009)
23. L.C. Prinsloo, W. Barnard, I. Meiklejohn, K. Hall, J. Raman Spectrosc. **39**, 646 (2008)
24. M. Maguregui, U. Knuutinen, K. Castro, J.M. Madariaga, J. Raman Spectrosc. **41**, 1110 (2010)
25. O. Cristini, C. Kinowski, S. Turrell, J. Raman Spectrosc. **41**, 1120 (2010)
26. H.G.M. Edwards, P.S. Middleton, M.D. Hargreaves, Spectrochim. Acta, Part A, Mol. Biomol. Spectrosc. **73**, 553 (2009)
27. M. Perez-Alonso, K. Castro, I. Martinez-Arkarazo, M. Angulo, M.A. Olazabal, J.M. Madariaga, Anal. Bioanal. Chem. **379**, 42 (2004)
28. K. Zehnder, Environ. Geol. **52**, 395 (2007)
29. S. Bioletti, R. Leahy, J. Fields, B. Meehan, W. Blau, J. Raman Spectrosc. **40**, 1043 (2009)
30. D. Bersani, P.P. Lottici, F. Vignalil, G. Zanichelli, J. Raman Spectrosc. **37**, 1012 (2006)
31. S.E.J. Villar, H.G.M. Edwards, J. Medina, F.R. Perez, J. Raman Spectrosc. **37**, 1078 (2006)
32. G. Van Hooydonk, M. De Reu, L. Moens, J. Van Aelst, L. Milis, Eur. J. Inorg. Chem. 639 (1998)

33. K. Castro, P. Vandenabeele, M.D. Rodriguez-Laso, L. Moens, J.M. Madariaga, Anal. Bioanal. Chem. **379**, 674 (2004)
34. V. Otieno-Alego, J. Hodgeman, D.C. Creagh, J. Am. Inst. Conserv. **40**, 35 (2001)
35. P. Baraldi, C. Fagnano, P. Bensi, J. Raman Spectrosc. **37**, 1104 (2006)
36. D. Wise, A. Wise, J. Raman Spectrosc. **35**, 710 (2004)
37. C. Frausto-Reyes, M. Ortiz-Morales, J.M. Bujdud-Perez, G.E. Magana-Cota, R. Mejia-Falcon, Spectrochim. Acta, Part A, Mol. Biomol. Spectrosc. **74**, 1275 (2009)
38. K. Castro, P. Vandenabeele, M.D. Rodriguez-Laso, L. Moens, J.M. Madariaga, Spectrochim. Acta, Part A, Mol. Biomol. Spectrosc. **61**, 2357 (2005)
39. K. Castro, M. Perez-Alonso, M.D. Rodriguez-Laso, J.M. Madariaga, J. Raman Spectrosc. **35**, 704 (2004)
40. P. Vandenabeele, F. Verpoort, L. Moens, J. Raman Spectrosc. **32**, 263 (2001)
41. P. Vandenabeele, T.L. Weis, E.R. Grant, L.J. Moens, Anal. Bioanal. Chem. **379**, 137 (2004)
42. M. Bowden, D.J. Gardiner, G. Rice, D.L. Gerrard, J. Raman Spectrosc. **21**, 37 (1990)
43. http://resources.renishaw.com
44. A. Bonifacio, C. Beleites, F. Vittur, E. Marsich, S. Semeraro, S. Paoletti, V. Sergo, Analyst **135**, 3193 (2010)
45. P. Mobili, A. Londero, G. De Antoni, A. Gomez-Zavaglia, C. Araujo-Andrade, H. Avila-Donoso, R. Ivanov-Tzonchev, I. Moreno, C. Frausto-Reyes, Rev. Mex. Fis. **56**, 378 (2010)
46. J. Vilnat, D. Bourgois, M. Dubois Applied, Spectroscopy **21**, 408 (1967)
47. R. Cesareo, F.W.V. Hase, Kerntechnik **15**, 565 (1973)
48. Z. Stosfertner, R.E.M. Hedges, R.D.G. Evely, Archaeometry **21**, 187 (1979)
49. C.S. Hogg, K.J. Burr, Trans. J. Br. Ceram. Soc. **81**, 129 (1982)
50. C.T. Yap, S.M. Tang, Appl. Spectrosc. **39**, 1040 (1985)
51. D. Radamacher, T. Shimotake, N. Bower, S. Peckham, Abstr. Pap. Am. Chem. Soc. **193**, 29 (1987)
52. R. Cesareo, F.V. Frazzoli, S. Sciuti, J. Radioanal. Nucl. Chem. **34**, 157 (1976)
53. D. Vaughan, Ind. Res. Dev. **24**, 144 (1982)
54. A. Longoni, C. Fiorini, P. Leutenegger, S. Sciuti, G. Fronterotta, L. Struder, P. Lechner, Nucl. Instrum. Methods Phys. Res., Sect. A, Accel. Spectrom. Detect. Assoc. Equip. **409**, 407 (1998)
55. R. Cesareo, G.E. Gigante, P. Canegallo, A. Castellano, J.S. Iwanczyk, A. Dabrowski, Nucl. Instrum. Methods Phys. Res., Sect. A, Accel. Spectrom. Detect. Assoc. Equip. **380**, 440 (1996)
56. P. Leutenegger, A. Longoni, C. Fiorini, L. Struder, J. Kemmer, P. Lechner, S. Sciuti, R. Cesareo, Nucl. Instrum. Methods Phys. Res., Sect. A, Accel. Spectrom. Detect. Assoc. Equip. **439**, 458 (2000)
57. G. Vittiglio, K. Janssens, B. Vekemans, F. Adams, A. Oost, Spectrochim. Acta, Part B, At. Spectrosc. **54**, 1697 (1999)
58. O. Williams-Thorpe, P.J. Potts, P.C. Webb, J. Archaeol. Sci. **26**, 215 (1999)
59. A.S. Serebryakov, E.L. Demchenko, V.I. Koudryashov, A.D. Sokolov, Nucl. Instrum. Methods Phys. Res., Sect. B, Beam Interact. Mater. Atoms **213**, 699 (2004)
60. C. Zarkadas, A.G. Karydas, Spectrochim. Acta, Part B, At. Spectrosc. **59**, 1611 (2004)
61. V. Desnica, M. Schreiner, X-Ray Spectrom. **35**, 280 (2006)
62. M. Ferretti, Nucl. Instrum. Methods Phys. Res., Sect. B, Beam Interact. Mater. Atoms **226**, 453 (2004)
63. J.L. Ferrero, C. Roldan, D. Juanes, E. Rollano, C. Morera, X-Ray Spectrom. **31**, 441 (2002)
64. S. Rohrs, H. Stege, X-Ray Spectrom. **33**, 396 (2004)
65. B. Newman, L. Loendorf, Plains Anthropol. **50**, 277 (2005)
66. F.P. Romano, G. Calvi, E. Furia, S. Garraffo, C. Marchetta, G. Pappalardo, L. Pappalardo, F. Rizzo, A. Rovelli, X-Ray Spectrom. **34**, 135 (2005)
67. F.P. Romano, G. Pappalardo, L. Pappalardo, S. Garraffo, R. Gigli, A. Pautasso, X-Ray Spectrom. **35**, 1 (2006)
68. G. Vittiglio, S. Bichhneier, P. Klinger, J. Heckel, W. Fuzhong, L. Vincze, K. Janssens, P. Engstrom, A. Rindby, K. Dietrich, D. Jembrih-Simburger, M. Schreiner, D. Denis, A. Lakdar, A. Lamotte, Nucl. Instrum. Methods Phys. Res., Sect. B, Beam Interact. Mater. Atoms **213**, 693 (2004)
69. D.N. Papadopoulou, G.A. Zachariadis, A.N. Anthemidis, N.C. Tsirliganis, J.A. Stratis, Talanta **68**, 1692 (2006)
70. G. Buzanich, P. Wobrauschek, C. Streli, A. Markowicz, D. Wegrzynek, E. Chinea-Cano, S. Bamford, Spectrochim. Acta, Part B, At. Spectrosc. **62**, 1252 (2007)
71. G. Buzanich, P. Wobrauschek, C. Streli, A. Markowicz, D. Wegrzynek, E. Chinea-Cano, M. Griesser, K. Uhlir, X-Ray Spectrom. **39**, 98 (2010)
72. K. Uhlir, M. Griesser, G. Buzanich, P. Wobrauschek, C. Streli, D. Wegrzynek, A. Markowicz, E. Chinea-Cano, X-Ray Spectrom. **37**, 450 (2008)
73. A. Deneckere, F.P. Hocquet, A. Born, P. Klein, S. Rakkaa, S. Lycke, K. De Langhe, M.P.J. Martens, D. Strivay, P. Vandenabeele, L. Moens, J. Raman Spectrosc. **41**, 1210 (2010)
74. J. Dik, K. Janssens, G. van der Snickt, L. van der Loeff, K. Rickers, M. Cotte, Anal. Chem. **80**, 6436 (2008)
75. B. Kanngiesser, W. Malzer, I. Reiche, Nucl. Instrum. Methods Phys. Res., Sect. B, Beam Interact. Mater. Atoms **211**, 259 (2003)
76. B. Kanngiesser, I. Mantouvalou, W. Malzer, T. Wolff, O. Hahn, J. Anal. At. Spectrom. **23**, 814 (2008)
77. I. Mantouvalou, K. Lange, T. Wolff, D. Grotzsch, L. Luhl, M. Haschke, O. Hahn, B. Kanngiesser, J. Anal. At. Spectrom. **25**, 554 (2010)
78. F.J. Hunter, J.G. Mcdonnell, A.M. Pollard, C.R. Morris, C.C. Rowlands, Archaeometry **35**, 69 (1993)
79. C. Fortina, A.S. Barbone, I.T. Memmi, Archaeometry **47**, 535 (2005)
80. S. Sotiropoulou, S. Daniilia, C. Miliani, F. Rosi, L. Cartechini, D. Papanikola-Bakirtzis, Appl. Phys. A, Mater. Sci. Process. **92**, 143 (2008)
81. P. Vandenabeele, R. Garcia-Moreno, F. Mathis, K. Leterme, E. Van Elslande, F.P. Hocquet, S. Rakkaa, D. Laboury, L. Moens, D. Strivay, M. Hartwig, Spectrochim. Acta, Part A, Mol. Biomol. Spectrosc. **73**, 546 (2009)
82. J. Zieba-Palus, M. Kunicki, Forensic Sci. Int. **158**, 164 (2006)
83. M. Bicchieri, M. Monti, G. Piantanida, A. Sodo, J. Raman Spectrosc. **39**, 1074 (2008)
84. K. Castro, A. Sarmiento, M. Maguregui, I. Martinez-Arkarazo, N. Etxebarria, M. Angulo, M.U. Barrutia, J.M. Gonzalez-Cembellin, J.M. Madariaga, Anal. Bioanal. Chem. **392**, 755 (2008)
85. S. Akyuz, T. Akyuz, S. Basaran, C. Bolcal, A. Gulec, Vib. Spectrosc. **48**, 276 (2008)
86. J. Striova, G. Coccolini, S. Micheli, C. Lofrumento, M. Galeotti, A. Cagnini, E.M. Castellucci, Spectrochim. Acta, Part A, Mol. Biomol. Spectrosc. **73**, 539 (2009)
87. C. Ricci, I. Borgia, B.G. Brunetti, C. Miliani, A. Sgamellotti, C. Seccaroni, P. Passalacqua, J. Raman Spectrosc. **35**, 616 (2004)
88. M. Aceto, A. Agostino, E. Boccaleri, F. Crivello, A.C. Garlanda, J. Raman Spectrosc. **37**, 1160 (2006)
89. T.D. Chaplin, R.J.H. Clark, M. Martinon-Torres, J. Mol. Struct. **976**, 350 (2010)
90. C.L. Aibeo, S. Goffin, O. Schalm, G. van der Snickt, N. Laquiere, P. Eyskens, K. Janssens, J. Raman Spectrosc. **39**, 1091 (2008)

91. K. Castro, S. Pessanha, N. Proietti, E. Princi, D. Capitani, M.L. Carvalho, J.M. Madariaga, Anal. Bioanal. Chem. **391**, 433 (2008)
92. K. Castro, N. Proietti, E. Princi, S. Pessanha, M.L. Carvalho, S. Vicini, D. Capitani, J.M. Madariaga, Anal. Chim. Acta **623**, 187 (2008)
93. L.C. Prinsloo, N. Wood, M. Loubser, S.M.C. Verryn, S. Tiley, J. Raman Spectrosc. **36**, 806 (2005)
94. G. van der Snickt, W. De Nolf, B. Vekemans, K. Janssens, Appl. Phys. A, Mater. Sci. Process. **92**, 59 (2008)
95. G. Paternoster, R. Rinzivillo, F. Nunziata, E.M. Castellucci, C. Lofrumento, A. Zoppi, A.C. Felici, G. Fronterotta, C. Nicolais, M. Piacentini, S. Sciuti, M. Vendittelli, J. Cult. Heritage **6**, 21 (2005)
96. A. Deneckere, W. Schudel, M. Van Bos, H. Wouters, A. Bergmans, P. Vandenabeele, L. Moens, Spectrochim. Acta, Part A, Mol. Biomol. Spectrosc. **75**, 511 (2010)
97. M. Sawczak, A. Kaminska, G. Rabczuk, M. Ferretti, R. Jendrzejewski, G. Sliwinski, Appl. Surf. Sci. **255**, 5542 (2009)
98. K.S. Andrikopoulos, S.X. Daniilia, B. Roussel, K. Janssens, J. Raman Spectrosc. **37**, 1026 (2006)
99. K. Castro, M. Perez-Alonso, M.D. Rodriguez-Laso, N. Etxebarria, J.M. Madariaga, Anal. Bioanal. Chem. **387**, 847 (2007)
100. K. Castro, B. Abalos, I. Martinez-Arkarazo, N. Etxebarria, J.M. Madariaga, J. Cult. Heritage **9**, 189 (2008)
101. L. Burgio, R.J.H. Clark, V.S.F. Muralha, T. Stanley, J. Raman Spectrosc. **39**, 1482 (2008)
102. M. Sendova, B. Kaiser, M. Scalera, V. Zhelyaskov, J. Raman Spectrosc. **41**, 469 (2010)
103. M. Maguregui, A. Sarmiento, I. Martinez-Arkarazo, M. Angulo, K. Castro, G. Arana, N. Etxebarria, J.M. Madariaga, Anal. Bioanal. Chem. **391**, 1361 (2008)
104. M. Maguregui, I. Martinez-Arkarazo, M. Angulo, K. Castro, L.A. Fernandez, J.M. Madariaga, Lasers Conserv. Artworks 177 (2008)
105. P.M. Ramos, I. Ruisanchez, K.S. Andrikopoulos, Talanta **75**, 926 (2008)
106. B. Vekemans, K. Janssens, L. Vincze, F. Adams, P. Vanespen, X-Ray Spectrom. **23**, 278 (1994)
107. A. Deneckere, L. de Vries, B. Vekemans, L. Van de Voorde, F. Ariese, L. Vincze, L. Moens, P. Vandenabeele, Appl. Spectrosc., submitted